

Seismic Computational Analysis of CFS-NEES Building

J. Leng¹, B.W. Schafer² and S.G. Buonopane³

Abstract

The objective of this paper is to explore computational modeling of a cold-formed steel framed building subjected to earthquake excitation. The selected two-story building will be subjected to full-scale motion on a shaking table in 2013 as part of the National Science Foundation funded Cold-Formed Steel – Network for Earthquake Engineering Simulation (CFS-NEES) project. The ledger-framed building employs load bearing cold-formed steel members throughout (wall, floors, and roofs) and employs OSB sheathed shear walls and an OSB sheathed diaphragm for the lateral force resisting system. Two- and three-dimensional analysis models capable of providing vibration, pushover, linear and nonlinear time history analysis are created in OpenSees. To date, the key nonlinearity investigated in the models is the characterization of the shear walls. The shear walls are either modeled as (a) elastic perfectly plastic, consistent with “state of the practice” level knowledge from AISI-S213 or (b) fully hysteretic with pinching and strength degradation based on shear walls tests conducted specifically for this building. The impact of the diaphragm stiffness is also investigated. Interaction of the lateral and gravity system, interaction of the joists, ledger, and walls, and the impact of openings on the diaphragm all remain for future work. The model is being employed to help determine the predicted experimental performance and develop key sensor targets in the response. In addition, the model will be used in incremental dynamic analysis to explore seismic performance-based design and sensitivity to model fidelity (2D, 3D, etc.) for cold-formed steel framed buildings.

¹ Graduate Research Assistant, Department of Civil Engineering, Johns Hopkins University, Baltimore, MD, USA (jleng1@jhu.edu)

² Professor and Chair, Department of Civil Engineering, Johns Hopkins University, Baltimore, MD, USA (schafer@jhu.edu)

³ Associate Professor, Department of Civil & Environmental Engineering, Bucknell University, Lewisburg, PA (sbuonopa@bucknell.edu)

Introduction

Lightweight cold-formed steel framing is a unique and effective building solution for low and mid-rise structures, but one in which much remains to be understood for the system to achieve its full efficiency and for modern performance-based seismic design methods to be fully enabled. The work presented herein is part of a National Science Foundation funded Cold-Formed Steel – Network for Earthquake Engineering Simulation (CFS-NEES) project that builds on single-story shear wall research to address multi-story cold-formed steel lateral force resisting systems. A key outcome of this project is to improve the analysis capabilities for complete cold-formed steel framed systems.

Analysis, in particular, the ability to accurately predict building deformations in modestly, moderately, and heavily damaged states under seismic excitations is a must for modern performance-based seismic design. However, current analysis methods in cold-formed steel design are nearly entirely member-based. Demands are largely based on assumed member tributary areas, end conditions are simplified to eliminate system interactions, and capacities are based on member-level only calculations. This approach has proven efficient and reasonably economic for current strength-based limit-states design methods, but it essentially cuts-off the future of system-level strength and reliability and seismic performance-based design. These new paradigms require more sophisticated system-level analysis models. Models that include all essential nonlinearities and are robust enough to provide meaningful predictions in damaged configurations are needed.

A significant focus of the seismic design community over the last decade has been the investigation of incremental dynamic analysis results for archetype structures. These models investigate the nonlinear dynamic performance of a structure against a suite of earthquakes with incrementally increased spectral acceleration. In much of this work the OpenSees (McKenna et al., 2011) structural analysis platform has been utilized. OpenSees is primarily a beam/frame element-based finite element code that includes a wide library of nonlinear hysteretic material models potentially appropriate for use in nonlinear time history analysis.

This paper provides the initial work of the CFS-NEES team to develop a nonlinear model appropriate for predicting the lateral response of the CFS-NEES archetype building: the CFS-NEES building. The models include essential nonlinearities related to the shear walls and provide a platform for investigating the full system performance, but much work remains to realize the analysis goals necessary for robust, modern performance-based design.

Description of the CFS-NEES building

The focus of this study is a professionally designed two-story cold-formed steel framed building, sited in Orange County, California (see Figure 1). Drawings, details, calculations and a complete narrative of the building design are available (Madsen et al. 2011). Gravity and lateral loads were determined per IBC (2009) which specifies ASCE 7-05. Cold-formed steel members were sized per American Iron and Steel Institute (AISI) Specifications (AISI-S100, -S210, -S211). The lateral force resisting system including shear walls and diaphragms were also designed using AISI specifications (AISI-S213).

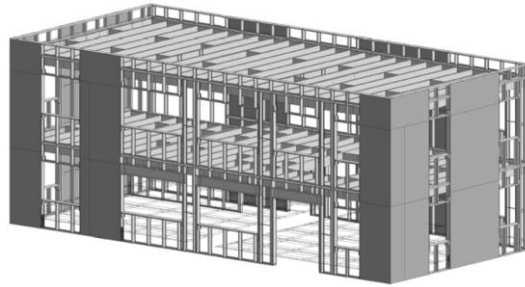


Figure 1 Three-dimensional BIM model of the CFS-NEES building, sheathing shown only for shear walls, south face is the long side of the building facing out

The building has a footprint of 23'0" x 49'9" and a height of 19'3". The gravity walls utilize an all-steel design philosophy (AISI-S211-07, AISI, 2007) and the members selected are 600S162-054 studs on the first floor and 600S162-033 studs on the second floor (nomenclature per AISI-S200). The joists are unblocked and utilize a continuously-braced design philosophy (AISI-S210-07, AISI, 2007), span the short direction of the building, with 1200S250-097 joists on the second floor and 1200S250-054 joists on the roof. The floors are ledger framed (hung) from the walls with a 1200T200-097 ledger, or rim track, capping the joists.

The selected lateral force resisting system uses OSB sheathed shear walls and diaphragms. For this system the response modification coefficient $R = 6.5$, overstrength factor $\Omega_0 = 3$, and deflection amplification factor $C_d = 4$. The Type I shear walls use back-to-back 600S162-054 chord studs, Simpson S/HDU6 holddowns, and 7/16 in. OSB fastened 6 in. o.c.. Length and location of the shear walls is designed to meet the base shear and architectural constraints resulting in the configuration provided in Figure 1. The diaphragm is modeled as flexible, per ASCE7-10, and 7/16 in. OSB 6 in. o.c. is utilized to meet the required strength. See Madsen et al. (2011) for details.

Nonlinear OpenSees models of the CFS-NEES building shear walls

The engineering model of the lateral force resisting system in a cold-formed steel framed building is that the primary energy dissipation occurs in designated shear walls. Shear walls are selected based on test data from a relatively wide body of research as compiled in AISI-S213-07. Based on the stud, sheathing, and fastener details AISI-S213 provides the shear capacity per unit length of the wall, v_n , and in addition provides a method for calculating the deflection of the shearwall, δ . Thus, the strength and stiffness (at least up to peak strength) are available in practice. Shear wall tests, e.g., as those completed for the CFS-NEES building as reported in Liu et al. (2012) can provide the complete nonlinear hysteretic response, including pinching and degradation over cycles.

A variety of modeling approaches exist for capturing shear wall nonlinearities in a model of a building. The work of van de Lindt et al. (2004 and 2010) is notable as it summarizes much of the extensive work that has been completed in modeling wood-framed, wood-sheathed, shear walls as well as complete buildings. Key insights on the importance of nonlinear deformations at fastener locations have proven remarkably useful in that context. In cold-formed steel framing, Martínez-Martínez and Xu (2011) demonstrated that using orthotropic plate elements for the shear walls and diaphragms can provide reasonable results and nice efficiencies. In addition, Shamim and Rogers (2012) provide specific modeling guidance for CFS framed shear walls utilizing steel sheet. The approach taken here is complementary to Shamim and Rogers.

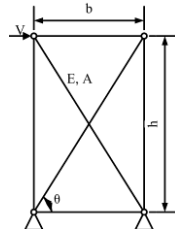


Figure 2 Illustration of shear wall model, diagonals are nonlinear

For the models investigated here the shear walls are treated, essentially, as a single degree of freedom: shear force V versus lateral deformation Δ . However, it is desired that the models have a physical width equal to their actual width in the building and that the forces in the chord studs develop similar to the typical truss analogy. A simple way to achieve this goal is to model the shear walls as a pin-connected panel with two diagonals as illustrated in Figure 2. The boundary members form a mechanism and the lateral stiffness and strength derives directly from the diagonals.

The axial force, F , in the diagonals that developed from shear force V is:

$$F = V / (2 \cos \theta) \quad (2)$$

where $\cos \theta = b / \sqrt{b^2 + h^2}$

Correspondingly, the stress in the diagonal (truss element) is

$$\sigma = F / A = V / (2A \cos \theta) \quad (3)$$

The axial strain (ε) in the diagonal is developed based on the lateral displacement of the shear wall Δ from:

$$e = d / l = D \cos \theta / \sqrt{b^2 + h^2} \quad (4)$$

Thus, with the preceding equations any nonlinear shear wall V - Δ relationship can be expressed as a nonlinear one-dimensional σ - ε relationship for the material in the diagonals, where:

$$\sigma = f(\varepsilon) \quad (5)$$

and function f is selected to match the desired V - Δ behavior. The two models explored for the shear walls are described in the following.

Elastic perfectly-plastic (EPP) state-of-the-practice shear wall model

Since strength and deflection up to peak are available in practice the most straightforward model for a shear wall is a simple elastic perfectly-plastic (EPP) model. Numerous variations on this model exist including the equivalent energy elastic perfectly-plastic model (see Liu et al. 2012) and others. However, in discussion amongst the authors and with the Industry Advisory Board for the CFS-NEES project it was decided that the simplest possible EPP model best characterizes current state-of-the-practice: set the “plastic” strength at the code specified nominal strength (V_n) and set the deflection (and thereby the stiffness) at the code specified deflection (δ) at the same V_n ; as shown in Figure 3a.

The nominal shear capacity per unit width, v_n , is found from AISI-S213 and for a given wall of width b the nominal shear capacity, $V_n = bv_n$. From Table C2.1-3 for 43 or 54 mil studs and track with 7/16 in. OSB on one-side and #8 fasteners spaced 6 in. o.c. $v_n = 825$ plf. (Note, this is the lower bound specified code

strength and is conservatively selected for the models developed here; further, this value must be reduced for walls with aspect ratios greater than 2:1). The deflection of the shear wall at v_n is provided by Equation C2.1-1 of AISI S213:

$$d(v_n) = \frac{2v_n h^3}{3E_s A_c b} + W_1 W_2 \frac{v_n h}{r G t_{sheathing}} + W_1^{5/4} W_2 W_3 W_4 \frac{\delta v_n \dot{\theta}^2}{\frac{b}{\theta}} + \frac{h}{b} d_{v_n} \quad (6)$$

All variables are defined in S213; briefly, the first term accounts for chord stud bending, the second term for shear in the sheathing, the third term is empirically fit to test data (and accounts for the bulk of δ) and the final term accounts for deformation at the hold downs. The V - Δ curve is converted into material properties for the diagonals in Figure 2 as described in the previous section.

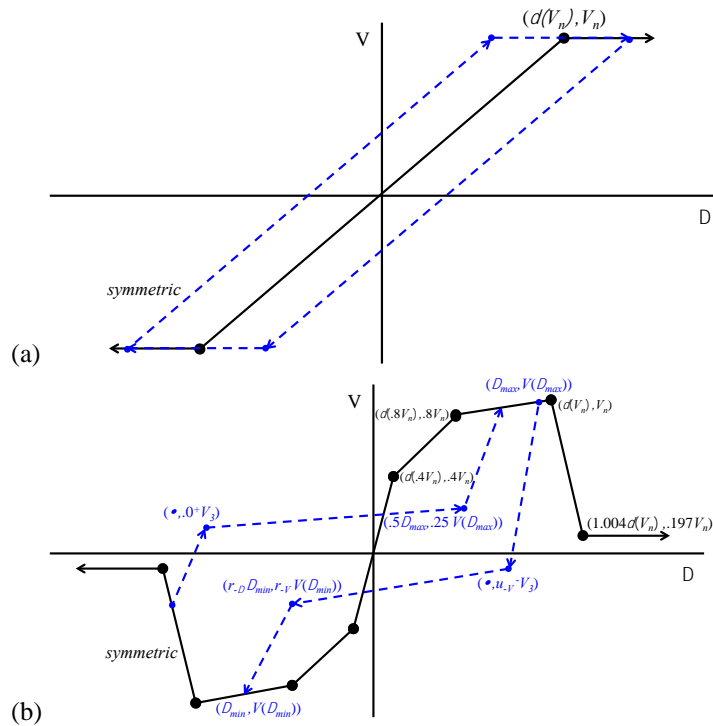


Figure 3 Nonlinear models for shear wall (a) EPP and (b) Pinching4

Pinching4 nonlinear hysteretic shear wall model

A far more realistic characterization of the shear wall behavior can be completed with the Pinching4 material (Lowe and Altoontash 2003) available in OpenSees. The model includes a four point backbone curve and a means to reduce (pinch) the response as a function of the maximum (+) or minimum (-) force or displacement experienced in a cycle as illustrated in Figure 3b. A complete discussion of parameterizing cyclic shear wall response with the Pinching4 model is available in Liu et al. 2012. Here the approach taken is to use the available data to augment the state-of-the-practice model.

As illustrated in Figure 3b the first three points in the backbone curve are set to $(\delta(0.4V_n), 0.4V_n)$, $(\delta(0.8V_n), 0.8V_n)$, and $(\delta(1.0V_n), 1.0V_n)$ and provide the pre-peak envelope as specified by AISI-S213. The last (fourth) point on the backbone curve is selected based on the average of Test 4 and 14 from Liu et al. (2012) and results in $(1.004\delta(1.0V_n), 0.197V_n)$. The pinching parameters (reloading and unloading) are also selected based on the average of reported results from Liu et al. (2012) and include: $r_{\Delta} = 0.5$, $r_V = 0.25$, and $u_V = 0.0$ as shown in Figure 3b. The $V-\Delta$ curve is converted into material properties for the diagonals in Figure 2 as described in the previous section.

Comparison of shear wall models with typical shear wall test

The developed EPP and Pinching4 models are compared to Test 12 of the shear wall tests of Liu et al. (2012) in Figure 4. The single story 8 ft x 9 ft OSB sheathed shear walls have the same details as the CFS-NEES building and are tested to the CUREE protocol.

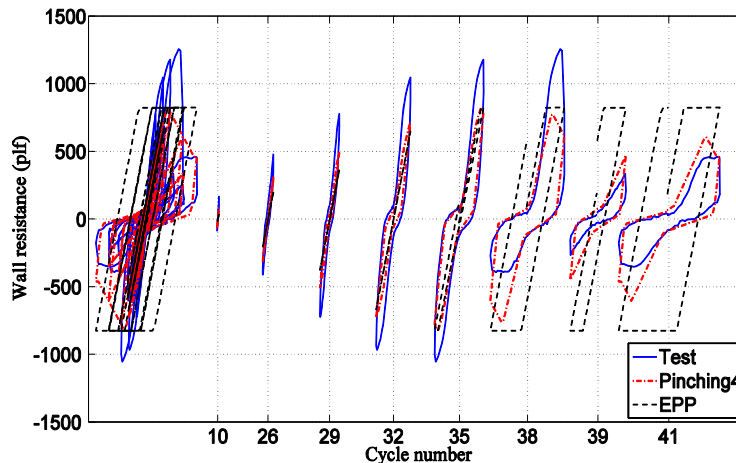


Figure 4 Pinching4 and EPP model compared with Test 12 of Liu et al. (2012)

In addition to showing the entire hysteretic response specific cyclic test loops are also provided in Figure 4; namely pre-peak loops 10, 26, 29, 32, and 35, the cyclic loop with maximum force: loop 38, and post-peak degraded loops: 39 (at 75% of the maximum deflection at peak load, loop 28) and 41 (at 150% of the maximum deflection at peak load).

The selected maximum capacity from AISI-S213 (825 plf) for the EPP and Pinching4 model is conservative when compared to the tests (a case can be made for a more aggressive selection from the tables of AISI-S213). Initial stiffness in the Pinching4 model is greater than the EPP model due to the use of δ at lower force levels in the first two branches of the Pinching4 model. The EPP model ignores pinching in the hysteretic behavior, near and past peak this assumption is untenable, as the actual response is severely pinched. The result is that the EPP model over-estimates the energy dissipation, in some cases grossly. (Note, as discussed in Liu et al (2012) equivalent energy elastic-plastic models sometimes referred to as EEEP models have the same drawback as the traditional EEP model in that they only match the energy of the backbone curve and ignore pinching, which is the dominant effect in the hysteretic response). Given these observations both the EEP and Pinching4 model of the shear walls are examined in the context of the CFS-NEES building.

Two-dimensional shear wall simulation

Two-dimensional (2D) models of the walls of the CFS-NEES building are constructed in OpenSees. The models, as depicted in Figure 5 for the North elevation, are meant only for lateral analysis and include only the shear walls as lateral resisting elements. The North elevation is highlighted as it has the largest shear force resistance.

The pinned connections designated in Figure 5 are realized by introducing coincident nodes and adding multi-point constraints that tie the translational degrees of freedom at the coincident nodes. The chord studs of the shear walls are modeled with actual cross-section properties, but since they are pinned they essentially do not participate in providing lateral resistance. The tracks (which here are a stand-in for the full diaphragm) are modeled using artificially increased material and cross section properties (1×10^5 times greater than tabled values of actual members) to transfer the shear force. All supports are pinned. Mass of each story is obtained from Madsen et al. (2011) and assigned to each

wall elevation proportional to shearwall widths. Lumped mass of each floor is located at the end of leaning column.

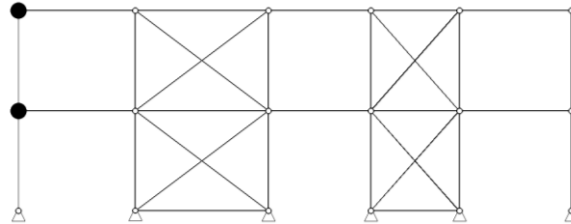
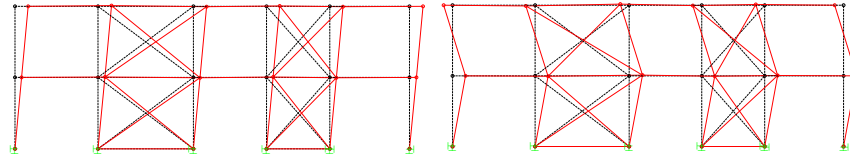


Figure 5 2D OpenSees model of CFS-NEES shear walls, North elevation

Free vibration analysis

Free vibration analysis was performed on the North elevation to check the natural periods and mode shapes. Figure 6 illustrates the first two mode shapes based on the EPP initial stiffness (i.e., secant stiffness to the peak strength). The periods are 0.552 seconds and 0.239 seconds and have less than four percent error compared with a simple Rayleigh quotient hand calculation. If the first branch linear stiffness of the Pinching4 model is used (i.e. secant stiffness to 40% of the peak strength), the periods reduce to 0.420 and 0.177 seconds. Note, even this is in relatively poor agreement with Equation 12.8-7 of ASCE 7-10 which yields a first mode period of 0.175 seconds. However, ASCE 7’s expression empirically includes more in the calculation than just the shear wall stiffness.



(a) First mode, $T_1 = 0.552$ seconds (b) Second mode, $T_2 = 0.239$ seconds
Figure 6 Mode shapes of North elevation model using EPP linear stiffness

Pushover analysis

Nonlinear pushover analysis is used extensively in seismic design and forms a key methodology in seismic design methods such as ASCE 41. Nonlinear pushover analysis of the North elevation is conducted in OpenSees. The results show that displacement control is needed for numerical stability. Currently, horizontal displacement of the control node, the node with lumped mass on the second floor, is set to 10% of the building height. This displacement is large enough for the shear elements to reach full capacity. Since the model does not include elements beyond the shear walls themselves little redistribution is observed and the results are essentially trivial (summation of wall capacities is

observed as expected). For verification and later use, a model without pinned connections is also created, and the base shear force is the same under pushover analysis.

Linear and nonlinear time history analysis

Elastic and nonlinear time history analysis of the North elevation of the CFS-NEES building is performed with both the EPP and Pinching4 (elastic models use only the first branch) shear wall models. Northridge earthquake measurements at Canoga Park (NGA0959) and Rinaldi receiving station (NGA1063) are selected as excitations. Based on the elastic response spectrum acceleration, one signal in a set is selected for analysis use. Signal 106 was selected for Canoga Park and used as the excitation in the long direction. Similarly, signal 228 was chosen for Rinaldi. The peak ground acceleration (PGA) of Canoga Park is 0.354 g, while it is 0.825 g for Rinaldi, illustrating significant difference between the records.

Currently, linear geometric transformation is used in the OpenSees model thus excluding nonlinear geometric (and P- Δ) effects. Rayleigh damping with damping ratios equal to two percent are adopted. Newmark average acceleration is used for integration in the dynamic analysis.

Time history of the first story drift for the EPP model normalized by the story height is provided in Figure 7. The Rinaldi ground motion causes permanent drifts greater than is expected to be sustainable by the building. Peak story drifts and peak shear forces are provided in Table 1 and Table 2 respectively. The EPP and Pinching4 models are compared with elastic models that have the same initial stiffness $K(V_n)$ for EPP per Figure 3a, and $K(0.4V_n)$ for Pinching4 per Figure 3b. Again the severity of the Rinaldi signal is underscored.

An estimate of the C_d , the displacement amplification factor, is provided in the last two rows of Table 1. Direct comparisons to ASCE 7 are highly approximate since the model has only limited nonlinearities included, only one elevation of the CFS-NEES building is included, and only two earthquake records at singular spectral acceleration levels are investigated. Nonetheless, it is somewhat instructive; design $C_d = 4$, and observed displacement amplifications vary from 0.7 to 3.5 in the EPP model and 1.6 to 4.8 in the more accurate Pinching4 model. The stronger Rinaldi input signal elicits higher displacement amplifications, and the displacement is largely concentrated in the first story.

Similarly, an estimate of R , the response modification coefficient, is provided in Table 2. The same provisos regarding the comparison to ASCE 7 as for C_d apply. Nonetheless the design value of $R=6.5$ may be loosely compared with the base

shear reductions of 2.2 and 2.8 for EPP and Pinching4 respectively under the Canoga Park signal and 4.0 and 4.8 for the Rinaldi signal. Though the predicted reductions are large, in the studied case, they are smaller than typically assumed in design.

Table 1 Peak first story and roof drift of North elevation in time history analyses

		Canoga Park, CNP 106		Rinaldi, RRS 228	
Model		Story1 <i>d</i> (in.)	Roof <i>d</i> (in.)	Story1 <i>d</i> (in.)	Roof <i>d</i> (in.)
Linear $K(V_n)$	$d_{K(V_n)}$	2.03	4.01	3.55	6.70
EPP	d_{EPP}	1.76	2.70	12.31	13.97
Linear $K(0.4V_n)$	$d_{K(0.4V_n)}$	1.37	2.68	2.31	4.51
Pinching4 (P4)	d_{P4}	4.00	4.20	11.04	11.04
Ratio to EPP	$d_{EPP}/d_{K(V_n)}$	0.87	0.67	3.47	2.09
Ratio to P4	$d_{P4}/d_{K(0.4V_n)}$	2.92	1.57	4.78	2.45

Table 2 Peak base shear force of North elevation in dynamic analyses

		Canoga Park, CNP 106	Rinaldi, RRS 228
Model		<i>V</i> (kip)	<i>V</i> (kip)
Linear $K(V_n)$	$V_{K(V_n)}$	37.12	65.27
EPP	V_{EPP}	16.50	16.50
Linear $K(0.4V_n)$	$V_{K(0.4V_n)}$	43.49	72.86
Pinching4 (P4)	V_{P4}	15.54	15.26
Ratio to EPP	$V_{K(V_n)}/V_{EPP}$	2.25	3.96
Ratio to P4	$V_{K(0.4V_n)}/V_{P4}$	2.80	4.77

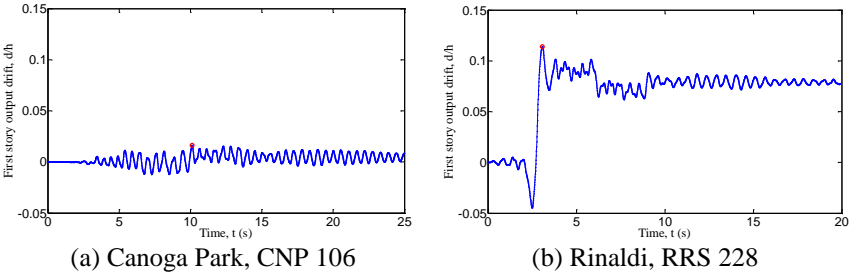


Figure 7 Nonlinear time history of first story drift using EPP material

Three-dimensional building simulation

Three-dimensional (3D) models of the CFS-NEES building, appropriate for lateral analysis only, are constructed in OpenSees, as depicted in Figure 8. The wall elevations are essentially the same as the 2D models; however, pinned connections in the corners of the shear walls are not employed. From a behavioral standpoint removing the pins allows bending to occur in the chord studs, which is realistic and of interest. From a practical modeling standpoint the use of coincident nodes (for modeling the pins) was not found to be compatible with rigid diaphragm modeling (which also employs multi point constraints). Two-dimensional models with and without pins were conducted, the total base shear capacities are identical and the stiffness increase by removing the pins is less than 10% in the first two modes (and modestly moves the predicted stiffness in the direction of the empirical ASCE 7 stiffness predictions). Note, the artificially stiff tracks used in the 2D models are replaced with beam-column elements using appropriate property values.

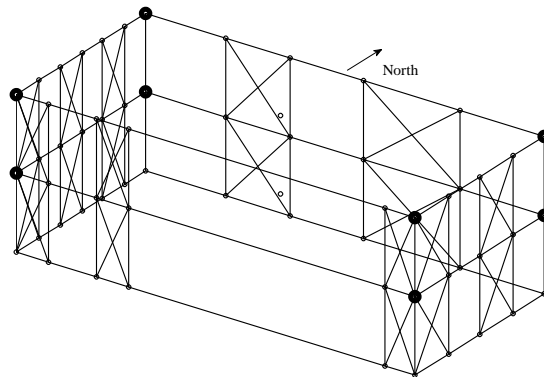


Figure 8 3D model of the building with rigid diaphragm

An important issue in the 3D model is the stiffness of the diaphragm. The building design (Madsen et al. 2011) assumes that the unblocked cold-formed steel joists with 7/16 in. OSB sheathing is flexible per Section 12.3 of ASCE 7-10. However, calculations with the diaphragm deflection expression in AISI-S213 indicate the diaphragm may have considerable stiffness. Further, expert opinion of the Industry Advisory Board for the CFS-NEES project was mixed on the issue and considered it still an open question. Exact characterization of the diaphragm stiffness will be left to system identification of the actual building during future testing. For now, it was decided to consider the two extremes in modeling: rigid diaphragm, and completely flexible diaphragm. Details of diaphragm openings, etc. are also not considered at this point.

In the model the mass of each story is divided equally and lumped to the four corners. This simple approximation will need refining in the future for a more exact prediction of the diaphragm rotational moment of inertia, P- Δ effects, and interaction of gravity and lateral loads.

Linear Static Analysis

An equivalent static lateral force of 300 kips is applied in the x (long, east-west) direction of the CFS-NEES building of Figure 8. The load is equally distributed to the four corner nodes and 1/3 to the first floor and 2/3 to the second floor. The vertical distribution is close to the first translational model shape. Table 3 provides the resulting base shear for the models under the two diaphragm assumptions. Both models show that the out of plane walls only carry a small fraction of the shear. The no-diaphragm model eliminates the load path between the North and South elevations and thus they carry close to the same shear force despite their significant difference in stiffness. The rigid diaphragm model results in over 2/3 of the total applied force being carried in the stiffer North elevation. Hand analysis performed in Madsen et al. (2011) shows a similar increase in the expected base shear of the North elevation, and also notes that this increased demand is not greater than the capacity of these walls.

Table 3 Base shear developed from 300 kip lateral force in long direction

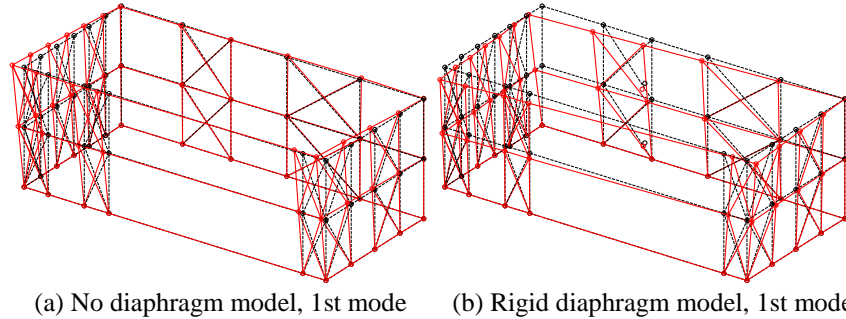
Elevation	No diaphragm model	Rigid diaphragm model
	Base shear (kips)	Base shear (kips)
North	151.15	206.40
South	124.48	78.40
West	12.50	7.82
East	11.87	7.39

Free vibration analysis

Free vibration analysis of the 3D model of the CFS-NEES building is conducted. The shear wall initial stiffness is based on the initial stiffness of the EPP model, i.e. $K(V_n)$ and both rigid and no (flexible) diaphragm models are considered. The first mode shape is reported in Figure 9 and the first six periods in Table 4. The rigid diaphragm model introduces torsion since the center of mass and center of stiffness are not aligned, as shown in Figure 9b. In addition, the rigid diaphragm models have modestly shorter periods than the no diaphragm models.

The 3D model has longer first mode periods than the 2D model and considerably longer than ASCE7 predictions when all the shearwalls, which are less stiff than North elevation, are included. Accurately assessing the building

period is important for properly characterizing the design spectra response and disagreement between the models and ASCE7 predictions underscores the importance of the experimental investigations that will soon be underway.



(a) No diaphragm model, 1st mode (b) Rigid diaphragm model, 1st mode
Figure 9 First mode shapes of 3D models

Table 4 Natural period comparison of two 3D models using $K(V_n)$ stiffness

Mode number	No diaphragm model	Rigid diaphragm model
	Period (sec)	Period (sec)
1	0.919 ^a	0.882 ^b
2	0.881	0.832
3	0.825	0.638
4	0.557	0.342
5	0.390	0.315
6	0.335	0.270

(a) for $K(0.4V_n)$, no diaphragm, mode 1 period = 0.817 sec.

(b) for $K(0.4V_n)$, rigid diaphragm, mode 1 period = 0.782 sec.

Linear and nonlinear time history analysis

Linear and nonlinear time history analysis is performed on the 3D model of the CFS-NEES building. Models with rigid diaphragm, no diaphragm, and EPP or Pinching4 shear wall idealizations are considered. The building is subjected to the Rinaldi excitation in the long (East-West) direction.

The input ground motion, second first floor story drift, and total base shear is provided for the nonlinear time history response of the rigid diaphragm model subjected to the Rinaldi excitation in Figure 10. The shear walls experience significant damage under this excitation. The Pinching4 model shows strong reductions in the base shear as the stiffness of the shear walls dramatically drop in the post-peak response, but concomitantly much greater story drift results in

the Pinching4 results. Regardless, peak story drift and peak base shear are directly correlated with the large pulse in the ground motion (PGA = 0.825g) at approximately 2.5 seconds. Comparison of linear and nonlinear time history results for peak story drift and peak base shear are provided in Table 5 and Table 6 respectively.

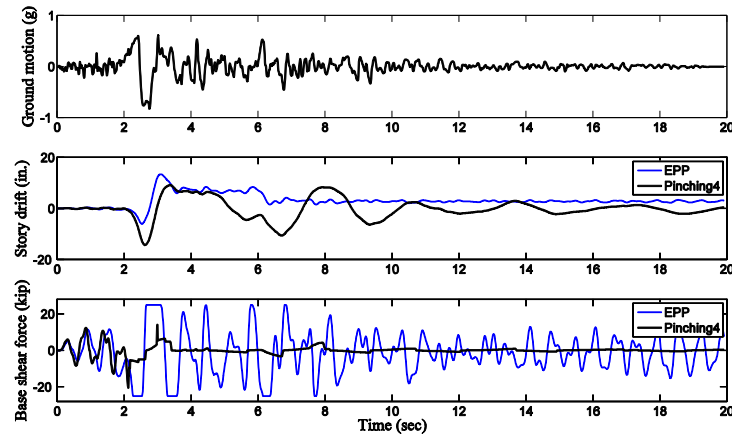


Figure 10 Time histories of Rinaldi ground motion (RRS 228), first story drift, and base shear for 3D model of CFS-NEES building, excitation in long direction

Table 5 Peak first story and roof center drift comparison of 3D models in dynamic analyses

		No diaphragm (D0)		Rigid Diaphragm (RD)		D0/ RD
		Story1 <i>d</i> (in.)	Roof <i>d</i> (in.)	Story1 <i>d</i> (in.)	Roof <i>d</i> (in.)	
Linear $K(V_n)$	$d_{K(V_n)}$	8.31	15.83	6.31	11.92	1.32
EPP	d_{EPP}	12.40	13.81	13.41	15.24	0.92
Linear $K(0.4V_n)$	$d_{K(0.4V_n)}$	5.81	11.50	3.69	6.74	1.57
Pinching4 (P4)	d_{P4}	12.59	13.05	14.29	14.52	0.88
Ratio to EPP	$d_{EPP}/d_{K(V_n)}$	1.49	0.87	2.13	1.28	0.70
Ratio to P4	$d_{P4}/d_{K(0.4V_n)}$	2.17	1.13	3.87	2.15	0.56

Table 6 Peak base shear force comparison of 3D models in dynamic analyses

		No dia- phragm (D0)	Rigid dia- phragm (RD)	D0/ RD
Model		V (kip)	V (kip)	
Linear $K(V_n)$	$V_{K(V_n)}$	143.33	154.36	0.93
EPP	V_{EPP}	29.60	30.55	0.97
Linear $K(0.4V_n)$	$V_{K(0.4V_n)}$	130.57	138.29	0.94
Pinching4 (P4)	V_{P4}	20.39	20.96	0.97
Ratio to EPP	$V_{K(V_n)}/V_{EPP}$	4.84	5.05	0.96
Ratio to P4	$V_{K(0.4V_n)}/V_{P4}$	6.40	6.60	0.97

Peak story drifts for the Rinaldi excitation, as recorded in Table 5, are significant – and although permanent story drifts are much smaller the nonlinear models essentially predict that all the first story shear walls are far into their collapse response (first story normalized drift is 13% to 15% depending on the model). Comparison of the no (flexible) diaphragm model with the rigid diaphragm model demonstrates a significant difference in the response between the linear and nonlinear shear wall idealizations. As provided in the last column of Table 5, in the linear models the deflections are greatest when the diaphragm is modeled as flexible; however in the nonlinear models this reverses as deflections are greatest when the diaphragm is rigid and the rigid diaphragm forces all first floor shear walls into greater damage.

Again, noting the provisos with comparisons to ASCE 7 as discussed in the 2D model results, the design $C_d = 4$, and observed displacement amplifications in the 3D models vary from 0.9 to 2.1 in the EPP model and 1.1 to 3.9 in the Pinching4 model. These 3D results are modestly reduced from the 2D model, but essentially aligned. (Note, the strongest wall was modeled in the 2D results).

For the Rinaldi excitation the drastic difference between linear and nonlinear force response is well highlighted by the difference in total peak base shear as reported in Table 6. Depending on the model details base shear from the nonlinear models is between 4.8 and 6.6 times less than linear analysis. For the Pinching4 model with rigid diaphragm, felt by the authors to be the most accurate characterization, the predicted base shear is 6.6 times less than the linear analysis. This may *very coarsely* be compared with the prescribed R factor of 6.5. The diaphragm assumption has little impact on the peak base shear as shown in the last column of Table 6; however, this is difficult to generalize as the excitation is large enough that all shear walls yield thus making the role of the diaphragm in distributing force to the shear walls irrelevant.

Comparison in the base shear response between the 2D (Table 3) and 3D models (Table 6) is illuminating. The ratio of nonlinear (P4) to linear peak base shear response in the 2D model is only 4.8, compared with 6.6 in the 3D model – for the same excitation. Thus, one can begin to understand how the system, and load sharing between shear walls, load sharing between different elevations, torsional influences due to diaphragm behavior, and the asymmetric distribution of shear walls, can result in differences in response not easily predicted by the 2D models.

Discussion and Future Work

The currently developed OpenSees models of the CFS-NEES building provides a platform for exploring the expected experimental behavior, demonstrates the importance of adequate nonlinear models and of employing three-dimensional models, but significant work remains.

Multidirectional seismic motions need to be considered. The record-to-record difference of earthquake ground motions can play a significant role in determination of failure modes. More specifically, the far-field ground motion data set suggested in FEMA P695 will be used along with incremental dynamic analysis (Vamvatsikos and Cornell, 2002) in the future.

At the global building scale the mass distribution needs to be handled in a finer manner and P- Δ effects, at least on the walls as a whole, need to be included.

The explored diaphragm models are adequate for bounding the solution, but a semi-rigid diaphragm model that includes differing stiffness parallel and perpendicular to the floor joists and incorporates the effect of openings is needed. AISI-S213 provides an approximation of the basic stiffness and preliminary models accounting for openings in the diaphragm have been explored.

The Pinching4 shear wall model is currently calibrated to a lower bound AISI S213 expected strength (V_n). Based on the Liu et al. (2012) testing a more precise model calibrated to the average test results can and will be developed. It is possible to separate the hold down flexibility from the test results and in the models, this separation will be completed so that the vertical flexibility at the chord stud locations is more accurately modeled. This is also beneficial so that the vertical flexibility between the first and second story shear walls can be included in the model.

In the walls, the lateral stiffness of the gravity system is currently ignored. Although the stiffness is less than the shear walls it is not zero as assumed in

current models. Final calibration of the gravity system contribution to the lateral system stiffness likely awaits the full-scale test results; however, the model can readily be adapted to include this stiffness. Challenges remain due to the lack of a clear load path in tension and limited/non-existent information on the nonlinear response of the gravity walls; but it is an important issue worthy of further consideration.

The impact of ledger framing is currently not explored in the existing models. Floor masses are not concentric, but rather hung from the interior studs and thus modestly eccentric. Interaction between the diaphragm and the shear wall as well as the gravity walls is assumed perfect in the existing models but in reality includes eccentricities and flexibilities that may have an important influence on response. Small scale testing is currently underway to explore some of the joist o ledger to stud (wall) response.

The impact of interior walls, interior gypsum, and the exterior insulated finishing system are obviously not included in current models, but will be examined in testing, and are worth incorporating in final models.

Rather than look at the model development as a series of improvements that must be made to re-create reality, the goal of the increasing model fidelity is to try to estimate the improved accuracy of response prediction and judge what level of fidelity is generally appropriate.

Conclusions

Computational models of the cold-formed steel framed two-story archetype building from the CFS-NES project, appropriate for lateral analysis, have been developed in OpenSees. The key nonlinearity targeted in the model is the response of the shear walls. State-of-the-practice models that incorporate an elastic perfectly-plastic idealization of the shear wall response are shown to be inadequate when compared with more advanced shear wall idealizations that include finer discretization of the overall backbone response and the influence of pinching and other hysteretic degradation, such as in the Pinching4 model of OpenSees. Two-dimensional models of the lateral response are generally adequate if the building diaphragm is flexible; however, they are inadequate for stiffer diaphragms. Even in a regular plan building such as the CFS-NEES archetype asymmetric distribution of the shear walls still leads to an eccentricity between the center of mass and center of stiffness that only a three-dimensional model with appropriate diaphragm stiffness appropriately captures. However, if excitations are strong enough the diaphragm stiffness is not as influential,

particularly for peak base shear. Significant future work remains to further the development of the computational model of the CFS-NEES buildings.

Acknowledgements

The authors are grateful to George E. Brown, Jr. Network for Earthquake Engineering Simulation (NEES) for the sponsorship. Thanks are extended to Rob Madsen in Devco Engineering for his design work of the archetype building. This paper was prepared as part of the U.S. National Science Foundation sponsored CFS-NEES project: NSF-CMMI-1041578: NEESR-CR: Enabling Performance-Based Seismic Design of Multi-Story Cold-Formed Steel Structures. The project also received supplementary support and funding from the American Iron and Steel Institute. Project updates are available at www.ce.jhu.edu/cfsnees. Any opinions, findings, and conclusions or recommendations expressed in this publication are those of the author(s) and do not necessarily reflect the views of the National Science Foundation, nor the American Iron and Steel Institute.

References

- American Iron and Steel Institute. (2007). North American specification for the design of cold-formed steel structural members, 2007 edition with supplement 2 (AISI S100-07 w/S2-10 ed.). Washington, DC: American Iron and Steel Institute.
- American Iron and Steel Institute. (2007). North American standard for cold-formed steel framing - general provisions, 2007 edition (AISI S200-07 ed.). Washington, DC: American Iron and Steel Institute.
- American Iron and Steel Institute. (2007). North American standard for cold-formed steel framing - floor and roof system design, 2007 edition (AISI S210-07 ed.). Washington, DC: American Iron and Steel Institute.
- American Iron and Steel Institute. (2007). North American standard for cold-formed steel framing - wall stud design, 2007 edition (AISI S211-07 ed.). Washington, DC: American Iron and Steel Institute.
- American Iron and Steel Institute. (2009). North American standard for cold-formed steel framing - lateral design 2007 edition with supplement no. 1 and commentary (AISI S213-07-SI-09 ed.). Washington, DC: American Iron and Steel Institute.
- American Society of Civil Engineers (ASCE). (2005). Minimum design loads for buildings and other structures (ASCE/SEI 7-05 ed.). Reston, Va: American Society of Civil Engineers.

American Society of Civil Engineers (ASCE). (2010). Minimum design loads for buildings and other structures (ASCE/SEI 7-10 ed.). Reston, Va.: American Society of Civil Engineers.

American Society of Civil Engineers (ASCE). (2007). Seismic rehabilitation of existing buildings (ASCE/SEI 41-06 ed.). Reston, Va.: American Society of Civil Engineers.

Applied Technology Council. (June 2009). Quantification of building seismic performance factors No. FEMA P695)

Liu, P., Peterman, K. D., Yu, C., & Schafer, B. W. (2012). Characterization of cold-formed steel shear wall behavior under cyclic loading for the CFS-NEES building. 21th International Specialty Conference on Cold-Formed Steel Structures - Recent Research and Developments in Cold-Formed Steel Design and Construction, St. Louis, MO.

Lowes, L. N., & Altoontash, A. (2003). Modeling reinforced-concrete beam-column joints subjected to cyclic loading. *Journal of Structural Engineering*, 129(12), 1686-1697.

Madsen, R. L., Nakata, N., & Schafer, B. W. (December 2011). CFS-NEES building structural design narrative No. CFS-NEES-RR01)

Martínez-Martínez, J., & Xu, L. (2011). Simplified nonlinear finite element analysis of buildings with CFS shear wall panels. *Journal of Constructional Steel Research*, 67(4), 565-575.

McKenna, F. et al. (2011). Open system for earthquake engineering simulation (OpenSees) (2.3.2 ed.) Pacific Earthquake Engineering Research Center, University of California, Berkeley, CA. Retrieved from opensees.berkeley.edu

Shamim, I., & Rogers, C. A. (2012). Numerical Modelling and Calibration of CFS Framed Shear Walls under Dynamic Loading. 21th International Specialty Conference on Cold-Formed Steel Structures - Recent Research and Developments in Cold-Formed Steel Design and Construction, St. Louis, MO.

Vamvatsikos, D., & Cornell, C. A. (2002). Incremental dynamic analysis. *Earthquake Engineering & Structural Dynamics*, 31(3), 491-514.

van de Lindt, J. W. (2004). Evolution of wood shear wall testing, modeling, and reliability analysis: Bibliography. *Practice Periodical on Structural Design and Construction*, 9(1), 44-53.

van de Lindt, J. W., Pei, S., Liu, H., & Filiatrault, A. (2010). Three-dimensional seismic response of a full-scale light-frame wood building: Numerical study. *Journal of Structural Engineering*, 136(1), 56-65.